



**HAL**  
open science

## Revisiting Battistini: Pleistocene coastal evolution of southwestern Madagascar

P. Boyden, Jennifer Weil-Accardo, Pierre Deschamps, N. Godeau, N. Jaosedy, A. Guihou, M.N. Rajaonarivelo, M. O'Leary, M. Humblet, A. Rovere

### ► To cite this version:

P. Boyden, Jennifer Weil-Accardo, Pierre Deschamps, N. Godeau, N. Jaosedy, et al.. Revisiting Battistini: Pleistocene coastal evolution of southwestern Madagascar. *Open Quaternary*, 2022, 8 (14), en ligne [17 p.]. 10.5334/oq.112 . hal-04564058

**HAL Id: hal-04564058**

**<https://hal.science/hal-04564058>**

Submitted on 16 May 2024

**HAL** is a multi-disciplinary open access archive for the deposit and dissemination of scientific research documents, whether they are published or not. The documents may come from teaching and research institutions in France or abroad, or from public or private research centers.

L'archive ouverte pluridisciplinaire **HAL**, est destinée au dépôt et à la diffusion de documents scientifiques de niveau recherche, publiés ou non, émanant des établissements d'enseignement et de recherche français ou étrangers, des laboratoires publics ou privés.



Distributed under a Creative Commons Attribution 4.0 International License



# Revisiting Battistini: Pleistocene Coastal Evolution of Southwestern Madagascar

RESEARCH PAPER

PATRICK BOYDEN

JENNIFER WEIL-ACCARDO

PIERRE DESCHAMPS

NICOLAS GODEAU

NICOLAS JAOSÉDY

ABEL GUIHOU

MAMY NIRINA RAJAONARIVELO

MICHAEL O'LEARY

MARC HUMBLET

ALESSIO ROVERE

\*Author affiliations can be found in the back matter of this article

]u[ubiquity press

## ABSTRACT

The study of paleo shorelines, particularly of those formed during the late Quaternary, provides robust insights into past climate variability. Advances in surveying techniques and chronological methodologies have dramatically improved the inter-comparability of regional and basin-wide paleo shoreline surveys. However, these advances have been applied unevenly across the globe. This is especially true in southwestern Madagascar, where, in the 1960s and 1970s, emerged Pleistocene beach and reef facies were first described in detail and dated to Marine Isotope Stage (MIS) 5a using U-Th alpha activity counting by french geologist René Battistini. Now, 50 years on, no further analysis of the coastal sequence has been made. In this study, we present an updated late Pleistocene coastal evolution model for the southwestern Madagascar coast. Utilizing a combination of Structure-from-Motion/Multi-View Stereo techniques and differential Global Navigation Satellite System surveys, we have created five high-resolution 3D outcrop reconstructions that have, in turn, been chronologically constrained using 10 U-series ages from both in situ and reworked coral samples. Our data suggest that the emerged reef was deposited during MIS 5e (~125 ka), then was covered by intertidal and beach sediment (including redeposited coral clasts of MIS 5e age), and finally capped off by thick eolianites. This sequence would suggest that the local sea level must have remained stable throughout MIS 5e in order to allow for the progradation of both the beach and reef environments.

## CORRESPONDING AUTHOR:

**Patrick Boyden**MARUM, University of Bremen,  
Germany[pboyden@marum.de](mailto:pboyden@marum.de)

## KEYWORDS:

Last interglacial; sea level;  
geomorphology; Madagascar;  
UAV surveying; U-series

## TO CITE THIS ARTICLE:

Boyden, P, Weil-Accardo,  
J, Deschamps, P, Godeau,  
N, Jaosedy, N, Guihou, A,  
Rajaonarivelo, MN, O'Leary,  
M, Humblet, M and Rovere,  
A. 2022. Revisiting Battistini:  
Pleistocene Coastal Evolution  
of Southwestern Madagascar.  
*Open Quaternary*, 8: 14,  
pp. 1–17. DOI: <https://doi.org/10.5334/oq.112>

## 1 INTRODUCTION

The accurate surveying and documentation of paleo shorelines, especially those formed in the late Quaternary, has become an integral part of understanding past climates (e.g., Dutton and Lambeck, 2012; Rovere et al., 2016) and putting ongoing and future sea-level rise in the context of the natural climate variability (e.g., Tierney et al., 2020). Large efforts have been directed towards describing, measuring, sampling, and dating geological proxies, with the aim of establishing the past positions of global mean sea level or to gauge the effects of post-depositional crustal motions caused by tectonics, glacial-isostatic adjustment, and, more recently, earth dynamic topography (Creveling et al., 2015; Dendy et al., 2017; Austermann et al., 2017).

In this context, some areas have received undoubtedly more attention than others from the geological community. For example, the Caribbean (Chen et al., 1991; Chutcharavan and Dutton, 2021), the Red Sea (Gvirtzman, 1994; Taviani et al., 2019), South America (Codignotto et al., 1988; Gowan et al., 2021), the Mediterranean (Hearty et al., 1986; Cerrone et al., 2021) or the Pacific (Chappell and Shackleton, 1986; Hallmann et al., 2021). Other areas, despite the abundant presence of geological indicators of Quaternary sea-level changes, have received relatively less attention. The western Indian Ocean is one such area. While it has been the focus of several early works (e.g., Alexander, 1969; Battistini, 1969, 1970; Montaggioni, 1972; Braithwaite et al., 1973; Battistini et al., 1976), it has been the subject of only three recent paleo-sea level studies, that utilized the most up to date surveying and chronological methods (Dutton et al., 2015; Vyverberg et al., 2018; Stephenson et al., 2019) to investigate paleo sea-level changes. Dutton et al. (2015) and later Vyverberg et al. (2018) analyzed fossilized coral deposits amongst the boulders of the granitic Seychelles, identifying slight mid-MIS 5e drop in relative sea level. Stephenson et al. (2019) resurveyed and re-dated fossil reef terraces on the northern tip of Madagascar that were originally described by Battistini (1965). This series of terraces, argue Stephenson et al. (2019), have been subject to post-depositional movement driven by mantle upwelling. Boyden et al. (2021) highlight that, while these are the only reliable sea-level datasets within the western Indian Ocean region, there are many other locations that would benefit from new field data, that may build upon the results of earlier works.

From the 1950s to the late 1970s, large efforts were made to document the geography and geology of the remote coasts of eastern Africa and the neighboring islands, including Madagascar. At the head of this charge was a then-young French geologist, René Battistini (1927–2017), who dedicated the majority of his career to unraveling the geomorphological, geological and ecological features present along the coasts of

Madagascar (e.g., Battistini et al., 1970; Battistini and Richard-Vindard, 1972). As part of his Ph.D. dissertation, Battistini (1964) mapped the southwestern coast of Madagascar, where he described emerged fossil Pleistocene coastal features (e.g., fossil coral reefs and cemented beach deposits), along with a succession of lithified dunes. From these features, Close to the small fishing village of Lembetabe, Battistini (1964) reported an emerged coral reef cropping out a few meters above modern sea level and attributed it to the Karimbolian, the Malagasy equivalent of the Eemian (Battistini, 1984). Battistini et al. (1976) and Battistini (1977) collected two samples from this reef, which were dated to  $85^{+4}_{-5}$  ka using the  $\alpha$ -counting U-Series technique, that was at that time, the state-of-the-art technique for dating Pleistocene corals (e.g., Barnes et al., 1956; Thurber et al., 1965). The southwest of Madagascar is a semi-arid landscape of rolling vegetated dunes and spiny forests, ideal conditions for carbonate preservation (Seddon et al., 2000). However, this desolate landscape also makes places such as the Lembetabe village difficult to access and logistically complex for geological fieldwork. As a result, after Battistini's work, this reef section was left unstudied for nearly 50 years. Here, we present the results of two geomorphological field campaigns in SW Madagascar. Through the use of modern geomorphological field techniques and high-precision U-series dating, we look to shed new light on the outcrop originally described by Battistini (1964, 1977).

## 2 METHODS

The two field campaigns were executed in May and October of 2019 to map the Quaternary coastal stratigraphy, previously described by Battistini (1964, 1977), at Lembetabe. We used differential Global Navigation Satellite System (GNSS) receivers and Structure-from-Motion/Multi-View Stereo (SfM-MVS) techniques applied to both unoccupied aerial vehicles (UAV) and land photographs to survey geological facies at high resolution and accuracy. Finally, fossilized corals, both in situ and reworked, were dated with high-precision MC-ICPMS U-series dating to establish a temporal context for the deposition of facies within this coastal section. This paper is accompanied by an online Electronic Supplementary Material where metadata, raw GNSS data, SfM-MVS quality reports, and additional visuals from the field are available at <https://doi.org/10.5281/zenodo.5727117> (Version 1.0, Boyden and Rovere, 2021).

### 2.1 STUDY AREA

The Mahafaly coast of southwestern Madagascar is physically dominated by the Eocene limestone of the broad, arid Mahafaly Plateau (Battistini, 1964; Du Puy and Moat, 1996). The western boundary of the plateau forms

an escarpment that runs NNW-SSE almost continuously for 280 km, from the town of Toliara (to the north) to Cap St. Marie (to the south). To the west of the cliff, the coastal plain is dominated by rolling semi-vegetated dune fields that either reach the coast or terminate atop several meters high Pleistocene bluffs. Carbonate sand pocket beaches occur exclusively along the coast except where the active dune fields overtop the predominantly Pleistocene bluffs. A combination of warm waters, limited terrestrial sediment input, and a narrow shelf allowed the development of fringing coral reefs. These reefs mark the southernmost extent of large reef development in the western Indian Ocean. Offshore, the predominant south to southwest deepwater swell propagates out of the Southern Ocean before breaking on the fringing reef.

This study focuses on the stretch of coastline fronting the small fishing village of Lembetabe. Situated approximately halfway between Toliara and Cap St. Marie, the coast is sheltered by a broad, shallow coral-dominated fringing reef flat. The reef is approximately 700 m wide on average, but it narrows to less than 100 m just south of the village (Figure 1). Starting at the

village and moving 5 km to the south, a well-preserved succession of Pleistocene coastal facies crops out from underneath Holocene and modern dune deposits.

## 2.2 SURVEY

The GNSS survey of the Pleistocene coastal facies at Lembetabe was carried out using a pair of Emlid REACH RS+ singleband GNSS receivers, set up in a Base/Rover Post-Processing Kinematic (PPK) workflow. While not ideal, due to the remote nature of Lembetabe there was no possibility to take advantage of receiving Real Time Kinematic (RTK) corrections through an NTRIP (Networked Transport of RTCM via Internet Protocol) service, nor via a permanent known base station broadcasting corrections over a LoRA (Long Range) radio. In order to obtain the most reliable results despite these shortcomings, the base station receiver was set up in an open area and left to collect data over each field day (approximately 12 hr, 24°40' 47.54841"S, 43°56' 36.13244"E, see processing reports available in the Electronic Supplementary Material). During the fieldwork, the base station collection point was moved to a fixed

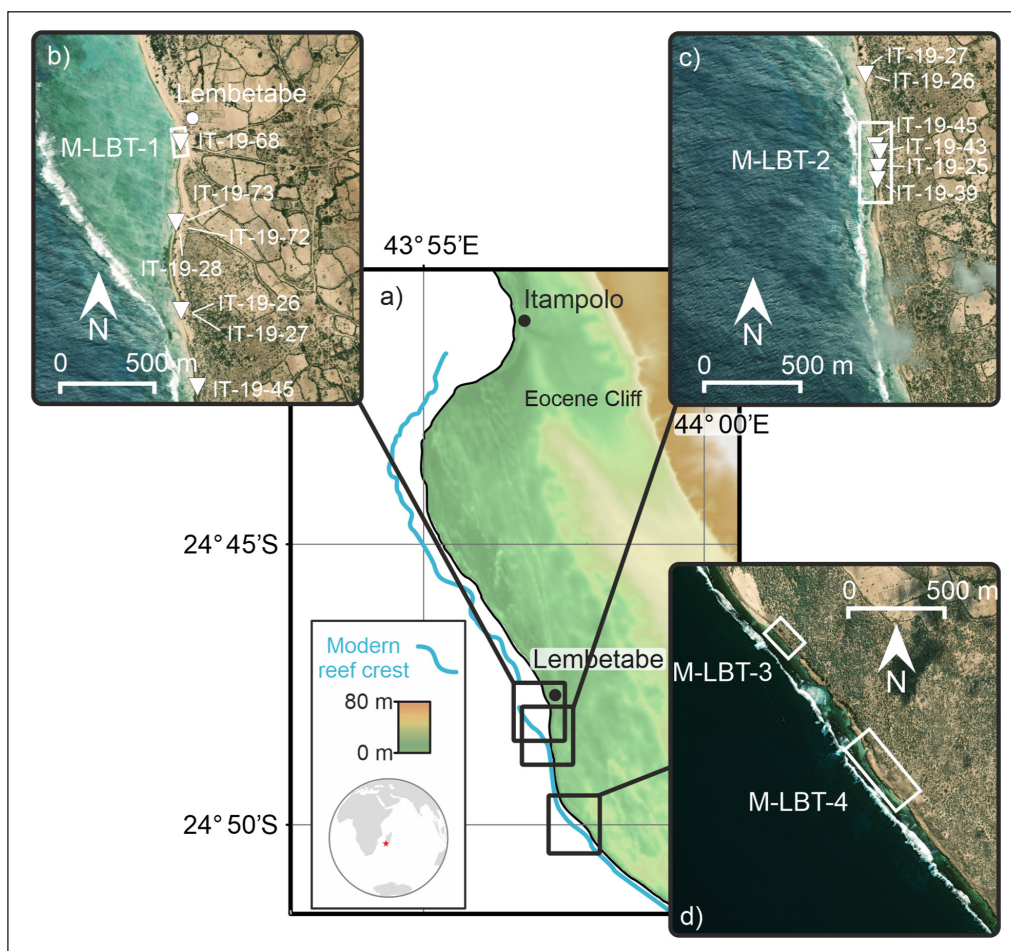


**Figure 1** (a) Map of southwestern Madagascar. (b) Fossilized reef flat (M-LBT-1) of the study area behind the broad shallow fringing reef in front of Lembetabe. (c) The main intertidal facies (M-LBT-2) (d) Paleo Backbeach and Eolianite Section, M-LBT-3 and M-LBT-4, respectively. Modern fringing reef crest is delineated by the light blue line, bathymetry contours in meters, and samples locations are identified by inverted triangles. Base DEM provided by AW3D (Japan Aerospace Exploration Agency). Satellite Imagery source: Esri, Maxar, GeoEye, Earthstar Geographics, CNES/Airbus DS, USDA, USGS, AeroGRID, IGN, and the GIS User Community.

position atop a tower and attached with zip-ties because of interference by free-ranging livestock. There, the base station was left to record continuously for approximately 23 hr, improving the  $1\sigma$  elevation accuracy from  $\pm 0.25$  m to  $\pm 0.15$  m.

At each field site, individual point collection was carried out using the Rover GNSS unit. In each instance, the Rover collected observations for approximately 5 min in a static position. Once back from the field, the raw observation logs (in RINEX format) from the Base Station were clipped by 1 hr to account for station initialization noise and then converted to a fixed point position using the online Canadian Spatial Reference System Precise Point Positioning (CSRS-PPP) tool provided by Natural Resources Canada (NRCan). For reference, CSRS-PPP outputs for each base station deployment are provided in the Electronic Supplementary Material. Then, utilizing the base station PPP-Fixed solution, the individual raw Rover logs were post-processed using RTKLIB (Version 2.4.3, [www.rtklib.com](http://www.rtklib.com)) to achieve the final individual survey-quality PPK positions.

Next, the GNSS elevations were converted from ellipsoid height to the modern mean sea level (MSL). To make this conversion, the MSL should be ideally observed regularly over an extended period, generally  $\geq 19$  yr, as well as the elevation above the ellipsoid established as a benchmark. However, no tide gauges are available in the vicinity of Lembetabe. Therefore, two INW PT2X Seametrics pressure transducers were deployed at the village of Itampolo, approximately 10 km north of the study area (Figure 1). One transducer was anchored to a dead coral colony in 1–2 m water depth, and the second was fixed onshore to record atmospheric pressure. The transducers were left to record continuously for 6 d at 1 min intervals. The elevation and position of each transducer were measured using the same GNSS workflow outlined above. To filter for any possible weather influence on the tidal measurements, the corrected tidal curve was then compared to the National Oceanic and Atmospheric Administration (2019) predicted tidal curve for Androka, approximately 30 km to the south, 25°04'S 44°07'E and Toliara, approximately 150 km to the north, 23°21'S 43°40'E. The resulting tidal curves and their respective MSLs were compared to the observed tidal curve and MSL at Itampolo (Electronic Supplementary Material Fig. A1). The predicted tidal curves from Androka and Toliara show good agreement with the timing of our tidal observations. While the overall amplitude of peak tidal stages at Androka and Toliara experience higher high tides and lower low tides, the root-mean-square-errors (RMSE) between respective tidal stage height at Itampolo is 0.286 and 0.292, for Androka and Toliara, respectively. Most importantly, the mean sea level calculated from the observations at Itampolo is 1.90 m a.m.s.l. This falls between the 1.99 m a.m.s.l. extracted from Androka conditions and

the 1.83 m a.m.s.l. at Toliara. Differences between the observed curve and the predicted curve are most likely a function of changes in local bathymetry and relative position within the Mozambique Channel, rather than hydrodynamic artifacts. Additionally, for the purposes of this study, the magnitude difference between mean tidal level and mean sea level is negligible and therefore treated as equal (Woodworth, 2017).

Finally, taking the resulting ellipsoidal – mean sea level difference, each survey point was corrected to MSL. The resulting errors for each individual GNSS point were propagated by calculating the quadrature of errors (Equation 1). Here the total elevation error ( $\sigma_E$ ) is calculated with  $\sigma_B$  as the GNSS Base Station error,  $\sigma_R$  as the GNSS Rover error,  $\sigma_B T$  as the GNSS Base Station error of the sea-level measurement, and  $\sigma_R T$  as the GNSS Rover error of the sea-level measurement.

$$\sigma_E = \sqrt{\sigma_B^2 + \sigma_R^2 + \sigma_{B_T}^2 + \sigma_{R_T}^2} \quad (1)$$

The same principle is applied to the calculation of the latitude and longitudinal errors with the MSL component simply omitted. Due to the overall temporal length of the Base Station observation, the resulting survey errors are dominated by the uncertainty of the Base Station, and in particular the mean base station elevation uncertainty. A summary of final point coordinates and associated uncertainties is provided in the Electronic Supplementary Material.

### 2.3 STRUCTURE-FROM-MOTION/MULTI VIEW STEREO

The application of SfM-MVS techniques to sequences of photographs collected with consumer-grade cameras, both on-land and mounted on UAVs, has been shown to provide accurate and reliable DEMs and 3D reconstructions of coastal morphology (e.g., Bistacchi et al., 2015; Casella et al., 2017; Bilmes et al., 2019). Here, we use both land-based, small-scale, SfM-MVS and unmanned aerial vehicle (UAV) based, large-scale, aerial SfM-MVS. Both land and aerial SfM-MVS follow the same general workflow, described below.

First, ground control points (GCPs) were arranged evenly throughout each respective target outcrop. The position of the GCPs was then collected using the GNSS system and workflow described in Section 2.2. Land-based photos were taken with a 20.1 megapixel Sony DSC-RX100M3 camera (8.8 mm focal length and resolution of  $5472 \times 3648$  pixels). Aerial photos were acquired using a DJI Mavic PRO UAV, equipped with a stock 12.35 megapixel camera (22 mm focal length and resolution of  $4000 \times 3000$  pixels), that was set at an angle of 90°. Each flight was piloted manually, keeping the drone at a speed of approximately  $1 \text{ ms}^{-1}$  and a constant altitude of 30 m. Flight tracks were flown to ensure the recommended minimum adequate overlap ( $\geq 90\%$ ).

Summary statistics of each photogrammetry project are provided in [Table 1](#). Photos were processed in Agisoft Metashape (Version 1.7.2, <https://www.agisoft.com>) to build DEMs and textured ortho-photomosaics. We followed the same workflow within Agisoft Metashape as Casella et al. (2017) for both the UAV and the land-based 3D outcrop reconstructions. Quality control reports of each reconstruction are provided in the Electronic Supplementary Material. Upper elevations of each unit were then extracted from the resulting 3D reconstruction in conjunction with field observations.

### 2.4 U-SERIES ANALYSIS

Along the exposed Pleistocene coast at Lembetabe, coral colonies in growth position, as well as coral rubble, were sampled when present. While in the field, we attempted to select the best preserved, unaltered corals for sampling based on physical appearance in order to exclude samples with clear signs of diagenesis. Once back from the field, before U–Th dating, mineralogical screening criteria were applied to identify coral samples that suffered postmortem diagenetic alteration. Initial mineralogical screening of collected samples was conducted using X-ray diffraction (XRD) on an X’PERT PRO machine following procedure and calibration equation established by Sepulcre et al. (2009).

The resulting screened samples were then processed using the following workflow to obtain U-series ages. After addition of a <sup>229</sup>Th–<sup>233</sup>U–<sup>236</sup>U spike calibrated against an aliquot of the Harwell HU-1 uraninite standard (see

Deschamps et al., 2012, for details), the sub-samples were dissolved in HNO<sub>3</sub>. U and Th fractions were separated and purified by column extraction chromatography using UTEVA resin. Analyses were conducted on an MC-ICPMS NEPTUNE PLUS following the procedure of Chiang et al. (2019). U–Th ages were obtained using Isoplot-R (Vermeesch, 2018) using the half-lives provided by Cheng et al. (2013) for <sup>230</sup>Th (75,584 yr) and <sup>234</sup>U (245,620 yr). Mineralogical analysis and U–Th dating was carried out at CEREGE, Aix-Marseille University.

### 3 RESULTS

Along the coast at Lembetabe, 118 GNSS points were taken in conjunction with four SfM-MVS projects located on our main outcrops (M-LBT-1 through M-LBT-4, [Figure 1](#)). The SfM projects capture six main units and are summarized in [Table 2](#). While these outcrops are noncontinuous, they form a segmented regressive stratigraphic sequence. The resulting units enable the cross-correlation of a depositional history. For readability, each outcrop is described hereafter as they occur moving southwards in the study area, starting at the village of Lembetabe at M-LBT-1 ([Figure 1](#)). Each outcrop section is supplemented by annotated orthomosaics along with interactive 3D reconstructions that are available online at Sketchfab <https://skfb.ly/o7CWB> along with additional outcrop photos in the Electronic Supplementary Material.

OUTCROP	MAIN FACIES	TYPE	NUMBER OF PHOTOS	RESOLUTION (mmPix <sup>-1</sup> )	TOTAL AREA (m <sup>2</sup> )	METASHAPE RMSE ERROR (m)
M-LBT-1	Reef Flat	Mixed	169	0.58	255	0.098
M-LBT-2	Intertidal	Land	856	0.315	159	0.502
M-LBT-2	Intertidal	Aerial	909	2.96	4500	0.638
M-LBT-3	Backbeach	Land	1071	0.329	161	0.317
M-LBT-4	Eolianite	Aerial	385	120	23500	0.700

**Table 1** Summary of SfM-MVS metadata. Further details are provided in outcrop individual report outputs from Metashape in the Electronic Supplementary Material.

UNIT	OUTCROP	MAIN FACIES	MEAN ELEVATION (m a.m.s.l.)
Unit 1	M-LBT-2	MIS 11 or younger calcarenite	2.8
Unit 2	M-LBT-1	Fossilized reef flat	2.1
Unit 3	M-LBT-1	Bioclastic infill pavement	2.2
Unit 4	M-LBT-1, M-LBT-2	Intertidal	5.2
Unit 5	M-LBT- 3, M-LBT-4	Back beach	4.0
Unit 6	M-LBT-3, M-LBT-4	Eolianite	6.8

**Table 2** Units and facies of the Lembetabe coast identified in this study. Mean elevations are the average upper unit extent extracted from SfM-MVS derived DEMs. Outcrop localities are provided in [Figure 1](#).

### 3.1 U-SERIES DATING

Ten samples were analyzed for U-series isotopic ratios. All of these coral samples showed calcite content below 1%. The only exception is the sample IT-19-25 that returned an averaged calcite content of  $1.95 \pm 0.13\%$  over three separate analyses. While this is greater than the 1% calcite content threshold used here, it is still below the 2% calcite content screening limit employed by others (e.g., Dutton and Lambeck, 2012; Hibbert et al., 2016).

The 10 U-Th ages obtained in this study and accompanying metadata are summarized in Table 3. They range from  $126.9 \pm 0.2$  ka to  $542 \pm 36$  ka. All following chronological uncertainties are reported in  $\pm 2\sigma$ . Measured  $^{230}\text{Th}/^{232}\text{Th}$  activity ratios were greater than the recommended value of 500, and all sample  $^{232}\text{Th}$  concentrations were well below the recommended concentration of 12 ppb (Chutcharavan and Dutton, 2021), preventing any need for detrital thorium correction in the final age calculation. Three samples returned last interglacial ages between  $126.9 \pm 0.6$  ka and  $128.6 \pm 0.6$  ka, with resulting  $\delta^{234}\text{U}_i$  values (between  $146.9 \pm 0.6$  and  $153.1 \pm 0.3$ ) falling within the acceptable  $147 \pm 5\%$  range defined for interglacial corals (see Hibbert et al., 2016). For the older samples,  $\delta^{234}\text{U}_i$  values show larger variations. Three samples with ages between 345 and 420 ka provide  $\delta^{234}\text{U}_i$  in agreement with the range generally accepted for interglacial seawater signature (IT-19-39,  $345.5 \pm 5$  ka,  $\delta^{234}\text{U}_i = 156.1 \pm 1.1\%$ ; IT-19-73,  $372 \pm 6$  ka,  $\delta^{234}\text{U}_i = 148.8 \pm 1.0\%$  and IT-19-43,  $419.9 \pm 12$  ka). These U-Th ages can be considered as relatively robust and allow to attribute these samples to MIS 11. The four samples that deliver the oldest ages (between 430 and 540 ka) have initial  $\delta^{234}\text{U}_i$  values significantly above this range ( $\delta^{234}\text{U}_i$  between  $200\%$  and  $300\%$ ). These higher  $\delta^{234}\text{U}_i$  values are indicative of open-system behavior as it is very unlikely that the ( $^{234}\text{U}/^{238}\text{U}$ ) seawater signature may have shifted up 50–150 d-unit in less than 100 ka after MIS 11. The diagenetic mechanism whereby  $^{234}\text{U}$  is added to the coral skeleton is generally accompanied by a  $^{230}\text{Th}$  enrichment (Gallup et al., 1994; Thompson et al., 2003; Villemant and Feuillet, 2003) leading to older apparent  $^{230}\text{Th}$  age. Taking into consideration this, it is plausible that these four samples are also MIS 11 in age.

### 3.2 LAST INTERGLACIAL FOSSILIZED REEF FLAT

The M-LBT-1 outcrop is located immediately south of the Lembetabe village (Figure 1b), and is the start of a bench that stretches approximately 1 km towards the south. The outcrop is mostly characterized by a well-preserved fossilized fringing reef flat, which was dated by Battistini (1972) to MIS 5a ( $85_{-5}^{+4}$  ka). Our first initial sample collected from this reef dated with U-series

suggests instead an MIS 5e age ( $127.5 \pm 0.5$  ka, IT-19-68). This reef composes what we called Unit 2 (Table 3 and Figure 2a). The lowest bed of this unit (0.7 m a.m.s.l) is characterized by a fine-grained, light-brownish to gray matrix with a minor component of micrite, solitary corals in growth position, and otherwise little to no bioclasts. This bed sits within the modern intertidal and has been eroded by low-energy wave action, that has created, on the modern reef, smooth decimeter-wide furrows that have been occupied by modern beach sediment (Figure 2d).

Moving upwards within Unit 2, the bioclastic component significantly increases in conjunction with a higher concentration of well-preserved corals colonies in growth position creating a robust framestone (Figure 2e, 2.1 m a.m.s.l). Articulated bivalves become abundant towards the top of this bed, which is then further infilled by bioclasts (Figure 2c). Based on the grain size and coral community, we interpret Unit 2 as a coral-dominated shallow-water reef sequence, similar to that found in the modern reef flat. Unit 3 shows apparent infilling of Unit 2, with a transition towards very coarse sand to granule grains, pink to light brown in color, predominantly sub-rounded to rounded, and well-lithified. Within Unit 3, there are significant millimeter-scale bioclasts, consisting of bivalve, gastropod shells, and isolated coral fragments. Two samples of coral rubble were taken from Unit 3 and dated to  $372.5 \pm 6$  (IT-19-72) and  $434 \pm 11$  ka (IT-19-73, Table 3). The component characteristics of Unit 3 are very similar to that of the modern beach. Topping off this section, Unit 4 represents a 20–30 cm thick layer of well-lithified, light brown medium sand calcarenite with little to no bioclast component. At M-LBT-1, the top of Unit 4 is flat (2.3 m a.m.s.l) and disappears under the modern dune. The bench created by Units 2, 3, and 4 continues south for approximately 1 km before disappearing completely under the modern dune. At the bench's furthest southern exposure, two neighboring pieces of coral rubble from Unit 4 were sampled at 4.2 m a.m.s.l and dated to  $128.6 \pm 0.6$  ka (IT-19-26) and  $126.9 \pm 0.6$  ka (IT-19-27, Table 3).

### 3.3 INTERTIDAL SEQUENCE

One kilometer south of M-LBT-1, a second outcrop (M-LBT-2, Figure 1c) was surveyed at a location where the modern backreef lagoon narrows to less than 100 m in width. At this location, the fossil reef sequence shrinks and eventually disappears, transitioning laterally to a sequence of intertidal calcarenites. At the base of this outcrop is Unit 1, a 3.5 m thick deposit of very well lithified medium to coarse-grained light pinkish-brown calcarenite. Within Unit 1 are sparse, decimeter-scale, coral-rubble that have been dated to MIS 11 ( $420 \pm 12$ : IT-19-4, and  $430 \pm 12$ : IT-19-45, Table 3). Distinctly different than the rest of the facies along the coastline,

SAMPLE ID	LATITUDE (°)	LONGITUDE (°)	ELEVATION (m a.m.s.l.)	UNIT	IN SITU (?)	<sup>238</sup> U (ppb)	<sup>232</sup> Th (ppt)	<sup>230</sup> Th (ppt)	[ <sup>234</sup> U/ <sup>238</sup> U]	[ <sup>230</sup> Th/ <sup>238</sup> U]	[ <sup>230</sup> Th/ <sup>232</sup> Th]	AGE (ka)	δ <sup>234</sup> U ‰
IT-19-25	-24.801424861	43.954153936	1.79 (0.27)	1	N	2644.0 (4.9)	34417.8 (80.4)	45.91 (0.09)	1.049 (0.002)	1.062 (0.003)	249 (1)	542.4 (36)	228.7 (4.0) <sup>a</sup>
IT-19-26	-24.797112989	43.953588405	4.20 (0.31)	4	N	2541.2 (4.8)	4131.7 (9.1)	32.33 (0.06)	1.106 (0.002)	0.778 (0.002)	1463 (4)	128.6 (0.6)	153.1 (0.3)
IT-19-27	-24.797112989	43.953588405	4.20 (0.31)	4	N	2818.6 (5.3)	6664.6 (13.5)	35.55 (0.07)	1.105 (0.002)	0.772 (0.002)	997 (3)	126.9 (0.6)	150.1 (0.3)
IT-19-28	-24.792153409	43.953087617	2.43 (0.31)	4	N	2286.0 (4.5)	310.6 (0.7)	39.70 (0.08)	1.054 (0.002)	1.062 (0.003)	23900 (72)	483 (22)	210.8 (2.1) <sup>a</sup>
IT-19-39	-24.801906971	43.954171558	0.78 (0.32)	4	N	2169.8 (7.2)	1043.3 (2.5)	36.66 (0.07)	1.059 (0.003)	1.034 (0.004)	6569 (20)	345.5 (5)	156.1 (1.1)
IT-19-43	-24.801177439	43.954201662	-0.87 (0.32)	1	N	2473.6 (8.4)	— <sup>b</sup>	42.48 (0.08)	1.053 (0.004)	1.051 (0.004)	— <sup>b</sup>	420 (12)	174.6 (1.5)
IT-19-45 <sup>c</sup>	-24.800581	43.954172	—	1	N	2156.0 (6.7)	2682.0 (6.2)	37.48 (0.07)	1.062 (0.003)	1.064 (0.004)	2613 (7)	430 (12)	206.8 (1.6) <sup>a</sup>
IT-19-68	-24.788422852	43.953324725	1.99 (0.24)	2	Y	2803.7 (8.3)	256.1 (0.5)	35.35 (0.06)	1.102 (0.003)	0.771 (0.003)	25814 (66)	127.5 (0.5)	146.9 (0.6)
IT-19-72	-24.792131112	43.953093846	1.97 (0.24)	3	N	3441.1 (9.3)	430.6 (0.8)	61.90 (0.10)	1.088 (0.003)	1.101 (0.003)	26878 (66)	434 (11)	299.7 (2.2) <sup>a</sup>
IT-19-73	-24.792158427	43.953090348	2.32 (0.24)	3	N	2221.3 (6.2)	11.3 (0.1)	37.59 (0.06)	1.052 (0.003)	1.035 (0.003)	620089 (5217)	372.5 (6)	148.8 (1.0)

**Table 3** U–Th ages of corals from Lembetabe. Values in parentheses are  $\pm 2\sigma$  absolute uncertainties. Square brackets denote activity ratios. Decay constants are  $9.1705 \times 10^{-6} \text{ yr}^{-1}$  for <sup>230</sup>Th,  $2.8221 \times 10^{-5} \text{ yr}^{-1}$  for <sup>234</sup>U (Cheng et al., 2013), and  $1.55125 \times 10^{-10} \text{ yr}^{-1}$  for <sup>238</sup>U (Jaffey et al., 1971). Ages are reported relative to the year of analysis, 2020, and do not include uncertainties associated with decay constants. All samples except IT-19-25 have <1% of calcite. Following XRD analysis, IT-19-25 returned an average calcite content of 1.95 (0.13)% based on three analysis.

<sup>a</sup> δ<sup>234</sup>U<sub>i</sub> well above recommended range for closed-systems, leading to possible older age bias in calculations (e.g., Chutcharavan and Dutton, 2021).

<sup>b</sup> IT-19-43 returned a <sup>232</sup>Th less than the [<sup>230</sup>Th/<sup>232</sup>Th] of our procedural blank and therefore the [<sup>230</sup>Th/<sup>232</sup>Th] was not calculated.

<sup>c</sup> IT-19-45 elevation measurement file was corrupted, therefore the backup handheld GNSS position was used and is presented at lower precision without an elevation.



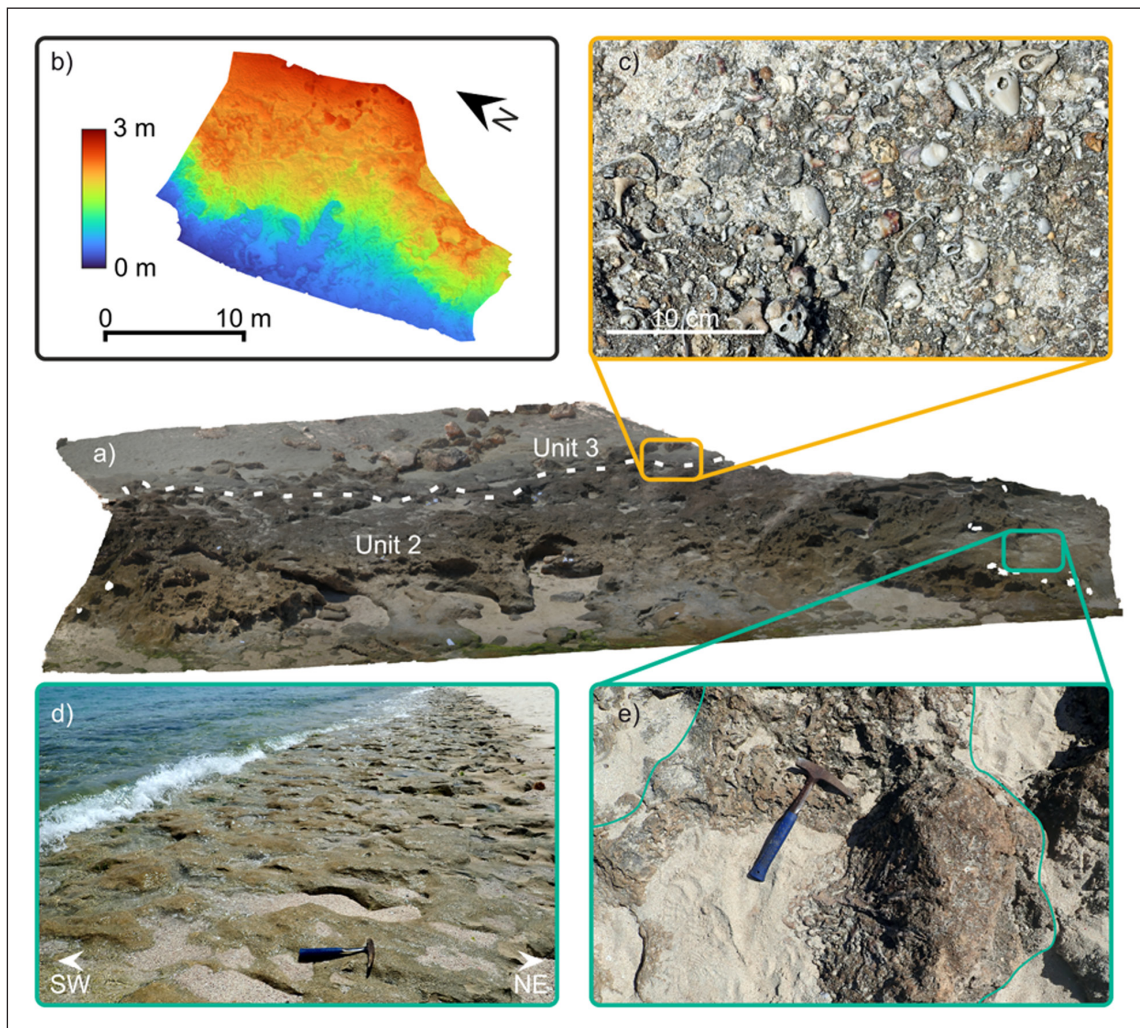


**Figure 2** (a) Fossilized fringing reef flat at M-LBT-1 (b) DEM of the M-LBT-1 outcrop. (c) Bioclasts of Unit 3 found on top of and infilling the fringing reef of Unit 2. (d) Modern decimeter-wide furrows that are commonly found within the upper modern intertidal zone located just to the north of M-LBT-1. (e) Sample IT-19-68 of well-preserved in situ *Pocillopora* fossil coral within Unit 2.

the lower surface of Unit 1 has been evenly weathered and therefore appears relatively smooth and tinted black in most places (Figure 3a, b).

As Unit 1 gradually slopes up, it transitions to Unit 4 at 2.8 m a.m.s.l. Unit 4 is a coarse calcarenite of grayish brown color that is approximately 1.2 m thick and less lithified than the underlying unit. Here, two samples of coral rubble were taken and dated to  $345.5 \pm 5$  and  $483 \pm 22$  ka, IT-19-39 and IT-19-28 respectively (Table 3). Of particular geomorphic note, instances of heavily weathered furrows have been preserved within this lower bed of Unit 4, immediately north of M-LBT-2 (Figure 3e). Included within the lower bed of Unit 4 are several small sub-angular boulders (approximately 50 cm in scale) of laminar bedded pinkish-brown calcarenite. Following the boulder inclusions, the outcrop becomes near vertical as Unit 4 becomes brown in color and bioclasts become more frequent. At approximately 50 cm from the base of Unit 4, 1-2 layers rich in angular shell and corals fragments occur in horizontal

poorly-sorted beds across almost the entire exposure (4.0 a.m.s.l.). The bioclasts within these layers are dissimilar to the bioclasts in the rest of the unit, which are much smaller and more rounded (Figure 3c).

Approximately 20 cm above the bioclast-rich layers, there is a sharp contact to finely-bedded calcarenite at 4.2 m a.m.s.l. This bed is a light gray fine-grained calcarenite with little to no bioclasts, approximately 10 cm thick. Directly above this bed, there is then a sharp transition to brownish-gray, very coarse, sub-angular calcarenite with a minor component of the light gray fine grains from directly below (Figure 3d). Moving up in the section, the very coarse grains begin to disappear and there is a transition back to the fine-grained calcarenite. Here, however, there are traces of thin laminar bedding alternating between medium and fine grains. Unit 4 has been weathered relatively smooth and slopes gradually upwards before disappearing under medium, sub-angular boulders composed of calcarenite and the modern dune, at 5.2 m a.m.s.l.

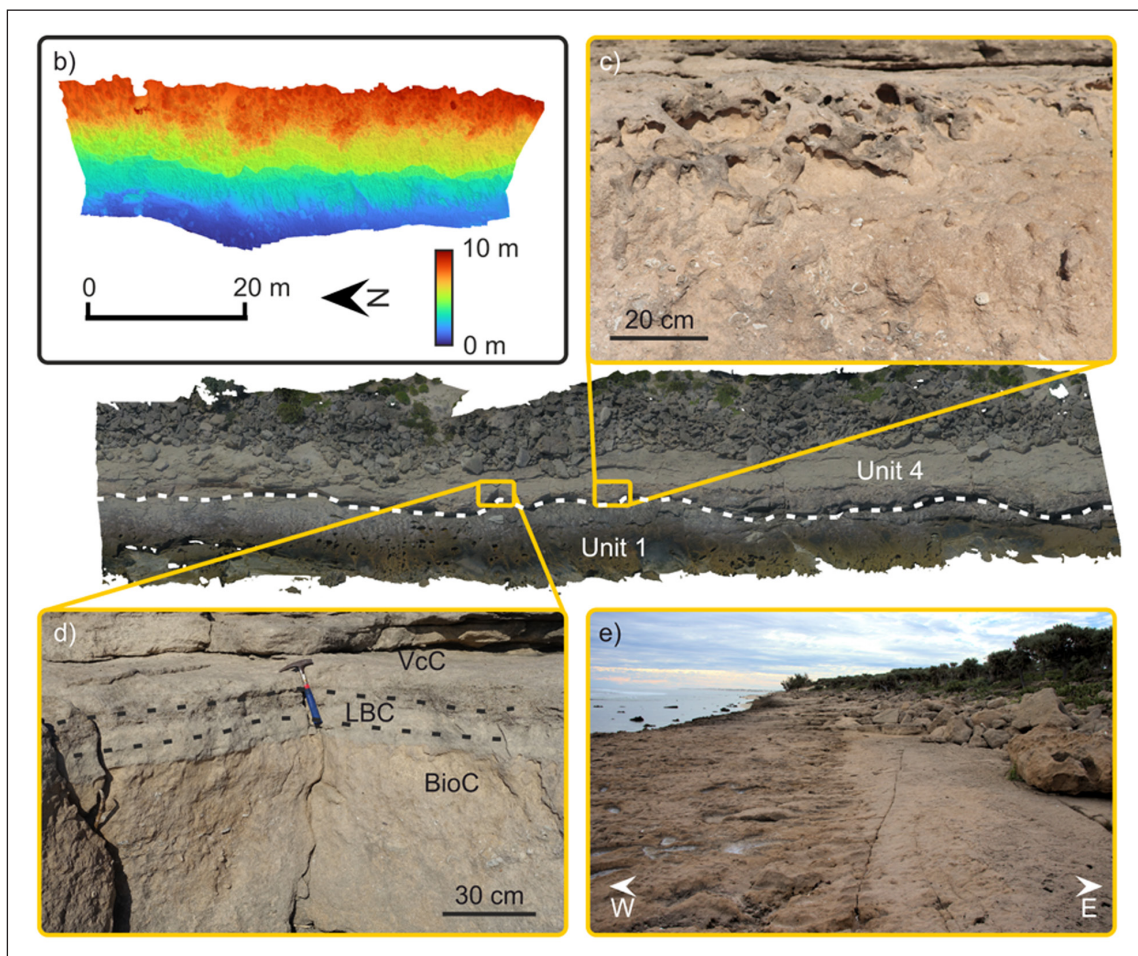


**Figure 3** (a) SfM-MVS derived orthomosaic of the intertidal section at M-LBT-2. (b) DEM of M-LBT-2. (c) Bioclasts, including coral fragments within the ‘swash zone’ of the intertidal zone. Note the relatively good preservation of shell fragments. (d) Transition from the bioclast layers of Unit 4 [BioC] to the fine-grained, parallel-bedded calcarenite [LBC] and the very coarse calcarenite on top [VcC]. (e) Heavily weathered paleo-furrows within Unit 4 and covering Unit 1, just to the north of the orthomosaic.

### 3.4 BACK BEACH AND EOLIANITE SEQUENCES

At the furthest southern extent of the study area, back beach facies and eolianites occur at two outcrops (M-LBT-3 & M-LBT-4, Figure 1d). From the modern shoreline to 4.0 m a.m.s.l, parallel to sub-parallel, horizontal bedded dark brownish-gray coarse calcarenite forms Unit 5 and represents a paleo-back beach environment. Similar to other sections of exposed calcarenite in the modern intertidal zone, the lower 1.5 m of this unit is heavily weathered and has a well-developed dissection surface, forming spires and razor-sharp ridges that surround large half-meter scale flat-bottomed pools. A combination of abrasion and chemical weathering has left the bedding only visible within pockets yet to be weathered (Figure 4c). At 2.9 m a.m.s.l, Unit 5 has been mostly eroded along bedding planes, leaving a relatively flat bench approximately 4 m wide (Figure 4a). The back of the bench is defined by an uneven vertical section that shows signs of subaerial weathering with the development of tafoni (Figure 4d). Exposed bedding planes, while weathered, show

a shallow, but distinct, landward dip. This landward dip is characteristic of the back beach environment where overwash has deposited sediment along the landward face of the beach berm (Nichols, 2009). Above Unit 5, a pinkish-brown, weakly lithified eolianite marks the transition to Unit 6 (Figure 4e).

The eolianite is continuously exposed moving further south, forming a broad bench and eroded unevenly by boulders being transported over the top of the cliff edge and to the foot of the modern dune (Figure 5a), as well as by subaerial exposure. Pinkish-brown in color, the eolianite is weakly lithified with moderate tafoni development. The eolianite contains infrequent decimeter-scale, sub-angular, bioclasts composed primarily of corals (Figure 5b). These specimens, however, were far too altered through diagenesis and therefore did not pass our initial screening for sampling. Additionally, at multiple locations, sub-angular clasts of grayish-brown, faintly parallel-bedded calcarenite are exposed and are similar in appearance to the intertidal facies of Unit 4 identified previously further north (Figure 5c).

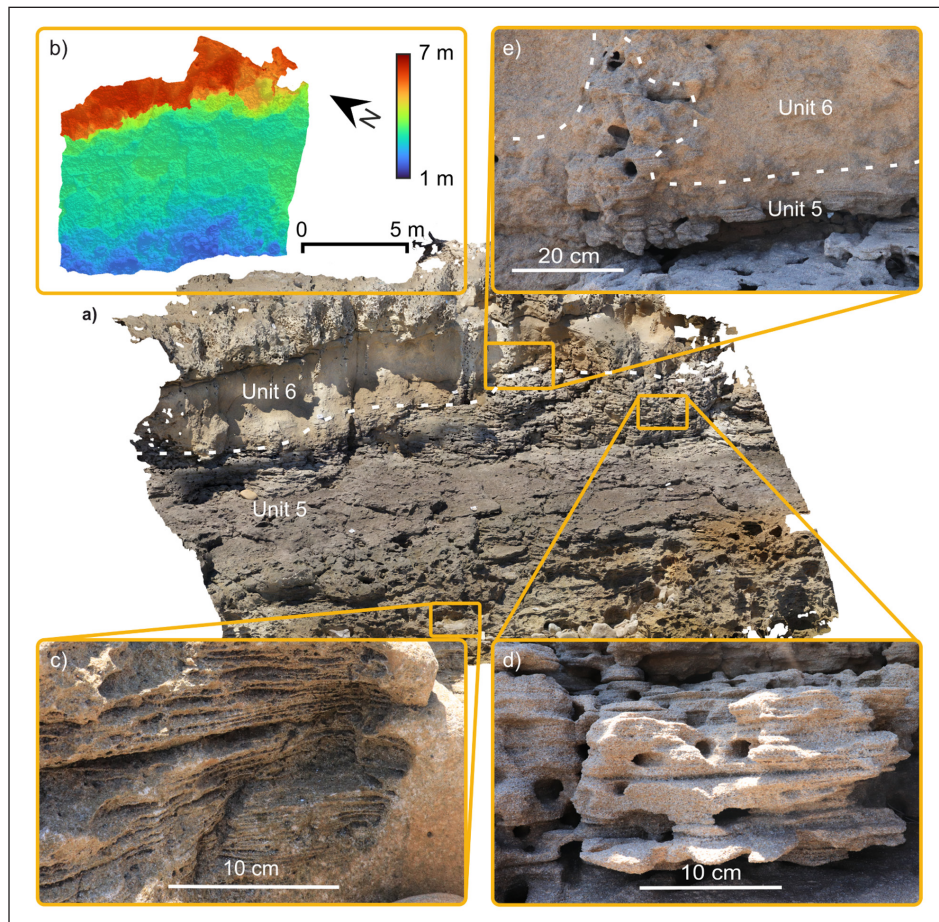


**Figure 4** (a) Backbeach and overlying eolianite at M-LBT-3. (b) DEM of M-LBT-3. (c) Modern shoreface of the laminar bedding of Unit 5. Mechanical and chemical weathering has left only pockets of bedding discernible. (d) Sub-aerial exposure of Unit 5 where tafoni have formed. (e) Soft contact between the laminar bedded Unit 5 and eolianite of Unit 6.

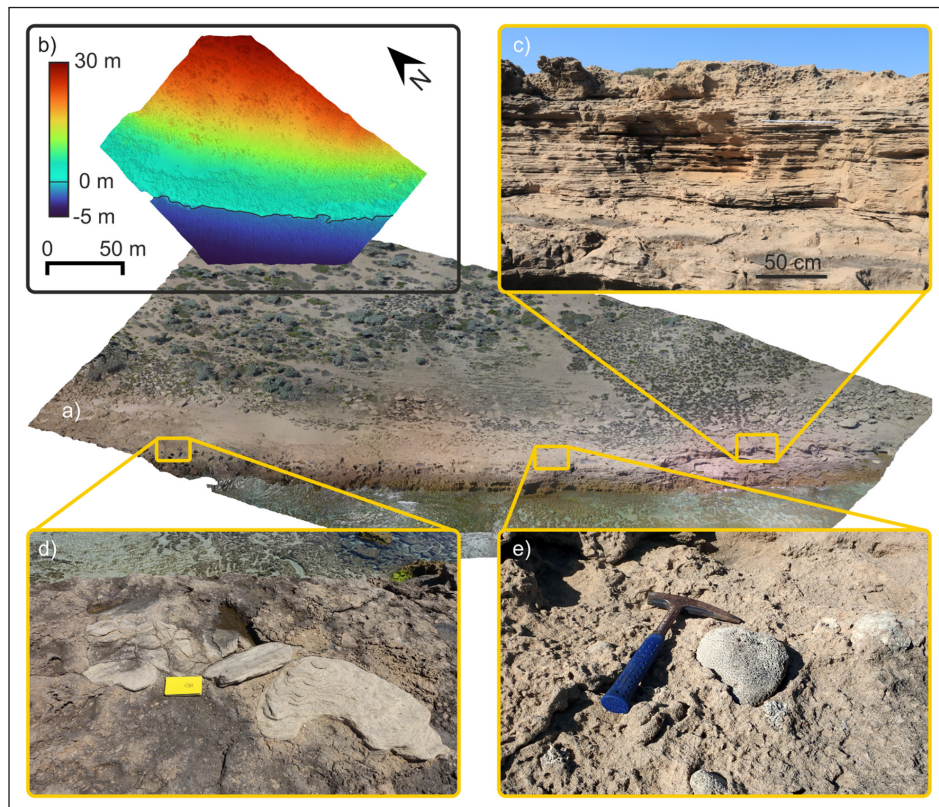


**Figure 5** (a) Eolianite bench at M-LBT-4. (b) DEM of M-LBT-4. (c) Laminar bedding of Unit 5 at M-LBT-4. (d) Sub-angular decimeter scale finely bedded intertidal clast within the eolianite, similar to Unit 4. (e) Decimeter scale coral rubble found within the upper part of the eolianite.

## 4 DISCUSSION

The Pleistocene coastal facies described in this study, together with the radiometric ages presented, allow for the reconstruction of the depositional history of the Lembetabe area in SW Madagascar. We surmise that the entire Pleistocene sequence observed in the study area is built upon a surface older than MIS 5, represented by Unit 1. While the coral samples from this unit are clearly not in situ (they may represent a coral rubble deposit), the sub-angular nature of the coral clasts within this old unit indicates a reasonably short duration of transport and subsequent sedimentation. This would therefore preclude multiple phases of reworking during interim interglacials (e.g., MIS 7). While the majority of samples display an initial uranium isotope ratio higher than seawater and are therefore treated as open-systems (e.g., Andersen et al., 2010), IT-19-25, IT-19-43, and IT-19-45 obtained from Unit 1 point to a possible formation during or after MIS 11 (420–370 ka). Eustatic sea-level proxies from South Africa point to a peak eustatic sea level of  $13 \pm 2$  m above present (Roberts et al., 2012). Such a peak in sea level, in conjunction with dynamic topography and glacial isostatic adjustment, would have allowed for the deposition of Unit 1 during either the transgressive or regressive phase of MIS 11 above modern sea level.

Battistini (1964) records an outcrop of an older beach calcarenite 4 m “above highest seas” at Cap Andrahomana (280 km to the southeast) and associates this to a former sea-level transgression, the Tatsimian (possibly MIS 11). This beach is subsequently covered by a +40 m thick sequence of well-lithified eolianites of the *Grande Dune* or “Large Dune”. The facies description of the beach calcarenite at Cap Andrahomana is quite similar to our observations of Unit 1, particularly the high level of lithification and pinkish brown color. Unfortunately, neither a corresponding paleo reef sequence for MIS 11 nor the intervening regressive *Grande Dune* deposit is exposed along this stretch of coastline, and therefore placing Unit 1 in a more detailed geomorphological and temporal context is challenging.

Through U-series dating, we correlate all the units deposited upon Unit 1 as formed during MIS 5e. In fact, while Unit 2 was previously dated to MIS 5a by Battistini (1972) ( $85_{-5}^{+4}$  ka), our new U-series analysis suggests instead a MIS 5e age ( $127.5 \pm 0.5$  ka; IT-19-68). The discrepancies between the two ages are most likely derived from differences in screening and analytic methodologies used. Unfortunately, the analytical metadata from Battistini (1972) is not readily available and therefore cannot be re-evaluated. In absence of such data, it remains difficult to evaluate the cause of the ~ 40 ka discrepancy between the old analyses obtained by  $\alpha$ -counting and our new age obtained by

mass spectrometry techniques. Additionally, this MIS 5a age at +1 m a.m.s.l for the Lembetabe outcrop is unlikely as MIS 5a eustatic sea level has been constrained to  $-8.5 \pm 4.6$  m (Creveling et al., 2017).

At peak MIS 5e sea level, the well-lithified calcarenite of Unit 1 was situated within the subtidal zone and deposition of the framestone represented by Unit 2, dated to  $127.5 \pm 0.5$  ka (IT-19-68), was initiated. This corresponds to a Pleistocene fringing reef and shows similar characteristics to the modern nearshore environment. Here, massive coral colonies are found in growth position. Drawing parallels to the modern fringing reef, the comparable size of coral colonies suggests that the paleo reef had reached a similar stage of reef development (Figure 6a). Furthermore, the environment represented by this reef is markedly different from the two drill cores taken from the barrier reef in front of the nearby town of Toliara, approximately 150 km to the north (Camoin et al., 2004). In those cores, the modern reef is overlaying heavily weathered Pleistocene reef slope deposits, at approximately 15 m below the modern reef and was dated between  $124.6 \pm 2.1$  ka and  $118.9 \pm 1.6$  ka (Camoin et al., 2004). This could place the reef crest, and the associated paleo shoreline, well landward of the core and possibly at a similar elevation to the paleo Lembetabe reef section. However, no emerged MIS 5e reef crest has been reported along the Toliara coast.

Unit 2 terminates at an erosional unconformity, creating a sub-horizontal bench that is characteristic of emergent reefs. The top of the reef is then infilled by Unit 3, which has a high bioclast component characteristic of a back reef/foreshore transitional environment (Figure 2c). Similar to the landward edge of the modern reef flat, coral and skeletal debris from the reef crest have been mobilized by wave action and then transported landward by overwash, finally being deposited at the beach-toe. This is in contrast to fore-reef deposits that are derived from sediment transported under return flow conditions interbedded with massive debris blocks from reef front slope failure (Montaggioni and Braithwaite, 2009).

The succession of facies suggests there was an influx of intertidal and beach sediment by the end of peak MIS 5e sea level. While the exact nature of beach accretion remains elusive, several reasonable contributors exist and others can largely be excluded. During the LIG, average global temperatures  $2^\circ\text{C}$  above present and simulated sea surface temperatures in the Southern Ocean during austral summer were  $2\text{--}3^\circ\text{C}$  above present (Yeung et al., 2021). In response to changes in global temperature gradients, wave climates and storm patterns have the potential to be different in the LIG. For example, modeling results presented by Yan et al. (2021) suggest that tropical cyclone activity in the North Atlantic was markedly different during the LIG, with shifts in areas of genesis and storm intensity

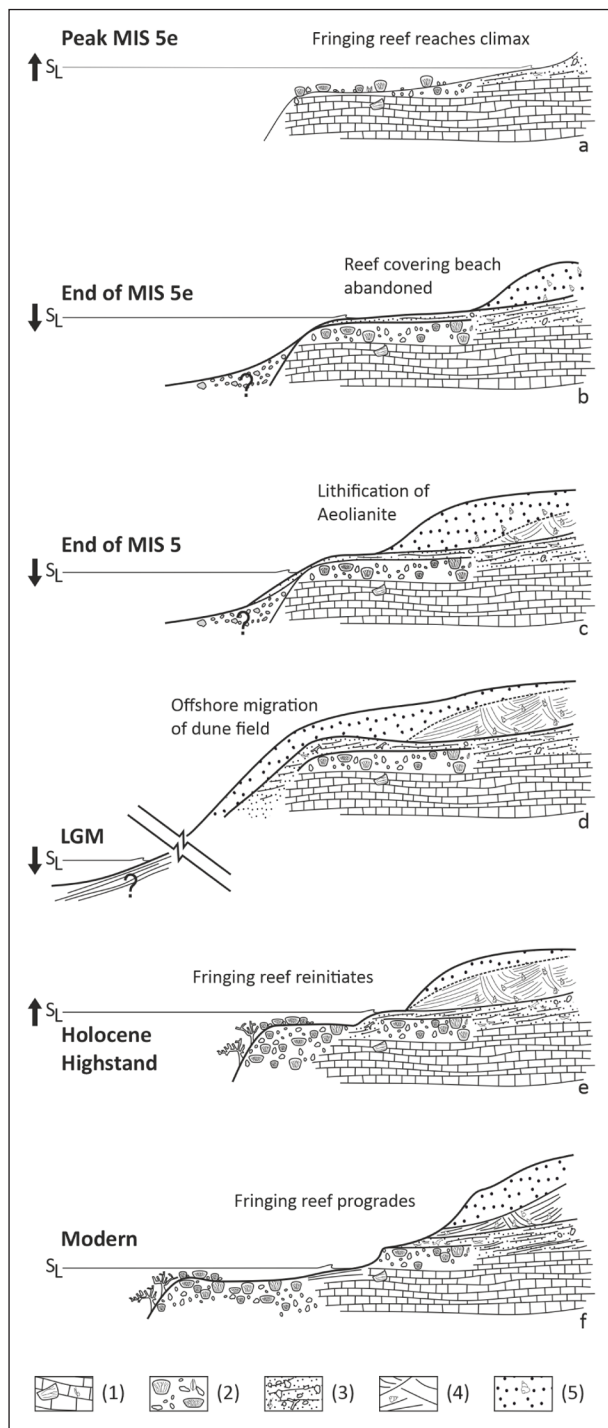


**Figure 6** Proposed morphological evolution of Lembetabe and the corresponding phases under Battistini (1964) in [brackets], **(a)** Start of MIS 5e High-stand [Karimbolian transgression], **(b)** End MIS 5e, **(c)** End of MIS 5, **(d)** Last glacial maximum [Lavanonian], **(e)** mid-Holocene High-stand [Flandrian transgression], **(f)** Modern. Generalized facies used in the figure and corresponding Units: (1) well-lithified early Pleistocene calcarenite (possibly MIS 11, Unit 1), (2) fringing reef (Unit 2), (3) beach sediments (Units 3–5), (4) eolianite (Unit 6), (5) mobile dune sediment.

driven by increases in sea surface temperature. While not applied to the Indian Ocean basin, a deviation from the modern wave and storm climate along the Lembetabe coast is conceivable and would have the potential to

rearrange sediment within the littoral system following peak MIS 5e peak sea level. Furthermore, increases in sediment production along the fringing reef and, in turn, increases in shoreward sediment transport, could have also contributed to net accretion of the paleo beach (e.g., [Cuttler et al., 2019](#)). On the other hand, changes to the hydrologic cycle and increases in riverine run-off from the Onilahy River (140 km to the north), the Linta River (30 km to the southeast), or the Menarandra River (70 km to the southeast) would also have the potential to contribute significantly more sediment to the littoral system. However, the limited siliciclastic component of Unit 4 and further decrease in precipitation over the South Africa monsoon region preclude a increase in terrestrial contribution ([Yeung et al., 2021](#)). Therefore, we surmise that some combination of changes in local wave climate and sediment production most likely took place by the tail end of MIS 5e in order to deposit the intertidal facies of Unit 4 along with reworked coral debris from Unit 2 (e.g., IT-19-26 and IT-19-27,  $128.6 \pm 0.6$  ka and  $126.9 \pm 0.6$  ka respectively, [Table 3](#)).

Once deposited, Unit 4 would have been readily lithified as beachrock while in the intertidal, undergoing subsequent weathering once exposed and leaving behind the weathered paleo-furrows seen in Unit 4 ([Figure 3e](#)). The basement of SW Madagascar is primarily Eocene carbonates, covered by dune deposits ([Besairie, 1973](#)). This limestone basement provides ample carbonate to be mobilized within what little groundwater outflow there is, readily precipitating beachrock ([Mauz et al., 2015](#)). A similar process is observed in the modern intertidal zone where relatively recent and weakly lithified beachrock is exposed and already has developed furrows ([Figure 2d](#)). The development of ridge-furrow systems in beachrock is driven by a combination of backwash and chemical weathering, suggesting that the paleo-furrows in Unit 4 represent a relatively stable period of sea level ([McLean, 1967](#)).

While the beachrock that is preserved in Unit 4, and its subsequent weathering pattern, would suggest a slow decrease in sea level during MIS 5e, other authors from elsewhere in the western Indian Ocean suggest the possibility of a second peak sea level at the end of MIS 5e. For example on Aldabra, situated at the northern end of the Mozambique Channel, [Braithwaite \(2020\)](#) suggest evidence of variations in sea level within MIS 5e. [Vyverberg et al. \(2018\)](#) also postulates the possibility of a stillstand or fall in sea level during the LIG on the main islands of the Seychelles. Such a reoccupation at the end of MIS 5e would also allow for the deposition of the beach-related facies above the reef at Lembetabe. However, robust proxies are still missing in the western Indian Ocean to confirm this hypothesis.

By the end of MIS 5, sea level began to rapidly fall and the beach was abandoned, allowing the beach dune (Unit 6) to begin over-topping the backshore ([Figure 6c](#)).

Incorporation of lithified, sub-angular boulders from Unit 4 (Figure 4c) and well-preserved coral clast (Figure 4d) tie the basin-ward advance of the eolianite to, at least, post-MIS 5e. The lack of significant structure development within the eolianite of Unit 6 also indicates a rapid basin-ward advance of the beach dune field. As sea level reached its lowest level during the LGM, 110–115 m below present in the Mozambique channel (Camoin et al., 2004), the Pleistocene section laid buried underneath eolianite and semi-mobile towering dune fields similar to what is observed in the modern hinterland (Figure 6d). Battistini (1964) identified this sequence as the *Petite Dune* or “Little Dune”, and is exposed regularly along the entire southwestern coast.

Following the LGM, sea level once again began to rise in the Mozambique Channel (e.g., Camoin et al., 2004). This would have forced the dune field to retreat and expose the weakly lithified eolianite to wave action and erosion. As the shoreline retreated, fringing reefs began to re-form in a similar pattern seen in the Toliara drill cores (Figure 6a, Camoin et al., 2004). While there is no direct evidence at Lembetabe, Battistini (1964) reports fossil tidal notches at 1–1.5 m above the modern notch at Baie des Assassins (310 km to the north) and Baie des Galions (300 km to the east, on the southeastern coast of Madagascar, near the town of Taolagnaro). The occurrence of notches above present sea level suggests the presence of the mid-Holocene high-stand in SW Madagascar, which could have brought the modern fringing reef at or near its current elevation as well as initiate the deposition of the recent beachrock seen in the modern intertidal.

## 5 CONCLUSIONS

In this study, we present new spatial and temporal constraints of geomorphological changes along the coast of SW Madagascar for the Late Pleistocene. Through the use of high-precision GNSS, SfM-MVS surveying techniques, and U-series (MC-ICPMS) dating, we show that:

1. The paleo reef flat section originally attributed to MIS 5a at Lembetabe (Battistini, 1972), should be instead attributed to MIS 5e.
2. The entire MIS 5e sequence lies upon an older unit, which is likely MIS 11 in age. While the depositional depth is unknown, this provides a marine limiting point at or after MIS 11 above present sea level.
3. The units recorded at Lembetabe show a clear regressive sequence, that spans the peak of MIS 5e sea level to the end of the last interglacial when the entire sequence was covered by dunes. This expands the temporal resolution previously reported by Battistini (1964) as the Karimbolian.

Refinements to the indicative meaning of the paleo reef at Lembetabe (i.e., the quantification of the paleo water depth at which the reef was formed), the age range of reef formation, the effect of glacial isostatic adjustment, and other local vertical land motions are essential to assess whether this area can be considered a reliable benchmark for MIS 5e global mean sea level and will be the objective of future work. In this perspective, this paper provides important building blocks to further evaluating paleo sea-level changes within the Indian Ocean and highlight the need for this broader area to i) revisit previously described outcrops with state-of-the-art techniques, and ii) expand the scope of Pleistocene coastal sites to include those in less accessible but ideally situated locations.

## DATA ACCESSIBILITY STATEMENT

3D reconstructions are available on Sketchfab at: <https://skfb.ly/o7CWB>. GNSS metadata, SfM-MVS reports, and additional outcrop photos are available in the Electronic Supplementary Material at <https://doi.org/10.5281/zenodo.5727117> (Version 1.0, Boyden and Rovere, 2021).

## ACKNOWLEDGEMENTS

The authors would like to acknowledge the IRD mission in Antananarivo, specifically Claude-Anne Gauthier, Regine Rakotoniaina, and Hary-liva Ravelonjatovo. We would also like to thank the support staff including drivers who made this remote fieldwork possible and finally, H el ene Mariot and Marion Defrance for their attentive support in CEREGE’s lab.

## FUNDING INFORMATION

This research was funded by the DFG (Deutsche Forschungsgemeinschaft) Excellence Cluster “EXC 2077: The Ocean Floor – Earth’s Uncharted Interface” (Project number: 390741603), the French National Institute for Sustainable Development (IRD), the Agence Nationale pour la Recherche (ANR, France) through the project EQUIPEX ASTER-CEREGE, the European Research Council (ERC) under the European Union’s Horizon 2020 research and innovation programme (grant agreement No. 802414), and the Helmholtz-Exzellenznetzwerke (grant No. ExNet-0001-Phase 2-3) “The Polar System and its Effects on the Ocean Floor (POSY)”.


## COMPETING INTERESTS

The authors have no competing interests to declare.


## AUTHOR CONTRIBUTIONS


PB, JWA, PD, and AR conceived the project; PB, JWA, PD, MNR, and AR planned the field campaign; PB, JWA, PD, NG, NJ, MO, and AR conducted field measurements and sample collection; PB analyzed both GNSS and SfM-MVS datasets; JWA, AG, and MH processed and analyzed U-series data; AR curated 3D outcrop visualizations on Sktechfab; PB wrote the initial manuscript; all authors reviewed and edited the manuscript.

## AUTHOR AFFILIATIONS


**Patrick Boyden**  [orcid.org/0000-0002-2757-7761](https://orcid.org/0000-0002-2757-7761)  
MARUM, University of Bremen, Germany

**Jennifer Weil-Accardo**  [orcid.org/0000-0002-3512-8536](https://orcid.org/0000-0002-3512-8536)  
CEREGE, Aix-Marseille University, Aix-en Provence, France


**Pierre Deschamps**  [orcid.org/0000-0003-1687-3765](https://orcid.org/0000-0003-1687-3765)  
CEREGE, Aix-Marseille University, Aix-en Provence, France


**Nicolas Godeau**  [orcid.org/0000-0003-4697-4938](https://orcid.org/0000-0003-4697-4938)  
CEREGE, Aix-Marseille University, Aix-en Provence, France


**Nicolas Jaosedy**  
CNRO, Hell-Ville, Nosy Be, Madagascar

**Abel Guihou**  [orcid.org/0000-0001-7347-378X](https://orcid.org/0000-0001-7347-378X)  
CEREGE, Aix-Marseille University, Aix-en Provence, France

**Mamy Nirina Rajaonarivelo**  
CNRO, Hell-Ville, Nosy Be, Madagascar

**Michael O'Leary**  [orcid.org/0000-0001-7040-3137](https://orcid.org/0000-0001-7040-3137)  
School of Earth Sciences, The University of Western Australia, Crawley, Australia

**Marc Humblet**  [orcid.org/0000-0002-8779-9948](https://orcid.org/0000-0002-8779-9948)  
Department of Earth and Planetary Sciences, Nagoya University, Nagoya, Japan

**Alessio Rovere**  [orcid.org/0000-0001-5575-1168](https://orcid.org/0000-0001-5575-1168)  
MARUM, University of Bremen, Germany; Department of Environmental Sciences, Informatics, and Statistics, Ca' Foscari University of Venice, Venice, Italy

## REFERENCES

- Alexander, CS.** 1969. Beach ridges in northeastern Tanzania. *Geographical review*, pp. 104–122. DOI: <https://doi.org/10.2307/213084>
- Andersen, MB, Stirling, CH, Zimmermann, B and Halliday, AN.** 2010. Precise determination of the open ocean <sup>234</sup>U/<sup>238</sup>U composition. *Geochemistry, Geophysics, Geosystems*, 11. DOI: <https://doi.org/10.1029/2010GC003318>
- Austermann, J, Mitrovica, JX, Huybers, P and Rovere, A.** 2017. Detection of a dynamic topography signal in last interglacial sea-level records. *Science Advances*, 3. DOI: <https://doi.org/10.1126/sciadv.1700457>
- Barnes, J, Lang, E and Potratz, H.** 1956. Ratio of ionium to uranium in coral limestone. *Science*, 124: 175–176. DOI: <https://doi.org/10.1126/science.124.3213.175.b>
- Battistini, R.** 1964. Etude géomorphologique de l'Extrême-Sud de Madagascar, Ph.D. thesis, University of Madagascar, Toulouse.
- Battistini, R.** 1965. Le Quaternaire littoral de l'Extrême Nord de Madagascar. *Bulletin d'Association française pour l'étude du quaternaire*, 2: 134–144. DOI: <https://doi.org/10.3406/quate.1965.991>
- Battistini, R.** 1969. Le Quaternaire du littoral kenyan entre Mombasa et Malindi. *Quaternaire*, 6: 229–238. DOI: <https://doi.org/10.3406/quate.1969.1136>
- Battistini, R.** 1970. Etat des connaissances sur les variations du niveau marin à Madagascar depuis 10.000 ans. *Comptes rendus Semaine géologique Madagascar*, pp. 13–15.
- Battistini, R, Guilcher, A and Marec, A.** 1970. Morphologie et formations quaternaires du littoral occidental de Madagascar entre maintirano et le Cap Saint-Andre. *Madagascar: Revue de Géographie*, 16: 45–81.
- Battistini, R.** 1972. L'hypothèse de l'absence de hauts stationnements marins quaternaires: Essai d'application à Madagascar et au sud-ouest de l'océan Indien. *Quaternaire*, 9: 75–81. DOI: <https://doi.org/10.3406/quate.1972.1194>
- Battistini, R and Richard-Vindard, G.** 1972. Biogeography and ecology in Madagascar. 21, The Hague, The Netherlands: Dr. W. Junk B.V. Publishers. DOI: <https://doi.org/10.1007/978-94-015-7159-3>
- Battistini, R.** 1977. Ages absolus 230Th/234U de dépôts marins Pleistocènes à Madagascar et dans les îles voisines. *Madagascar Revue de Géographie*, pp. 73–86.
- Battistini, R.** 1984. Mise au point sur la terminologie du Quaternaire malgache. *Madagascar (Tananarive)*, pp. 9–25.
- Battistini, R, Lalou, C and Elbez, G.** 1976. Datation par la méthode 230Th 234U du Pleistocène moyen marin de Madagascar et des îles voisines. *Bulletin de la Société Géologique de France*.
- Besairie, H.** 1973. Carte géologique a1:2000000 de Madagascar. Antananarivo, Service Géologique de Madagaskara.
- Bilmes, A, D'Elia, L, Lopez, L, Richiano, S, Varela, A, del Pilar Alvarez, M, Bucher, J, Eymard, I, Muravchik, M, Franzese, J, et al.** 2019. Digital outcrop modelling using “structure-from-motion” photogrammetry: Acquisition strategies, validation and interpretations to different sedimentary environments. *Journal of South American Earth Sciences*, 96: 102–125. DOI: <https://doi.org/10.1016/j.jsames.2019.102325>
- Bistacchi, A, Balsamo, F, Storti, F, Mozafari, M, Swennen, R, Solum, J, Tueckmantel, C and Taberner, C.** 2015. Photogrammetric digital outcrop reconstruction, visualization with textured surfaces, and three-dimensional structural analysis and modeling: Innovative methodologies applied to fault-related dolomitization (Vajont Limestone, Southern Alps, Italy). *Geosphere*, 11: 2031–2048. DOI: <https://doi.org/10.1130/GES01005.1>
- Boyden, P and Rovere, A.** 2021. Electornic Supplementary Material for “Revisiting Battistini: Pleistocene coastal evolution of Southwestern Madagascar”. DOI: <https://doi.org/10.5281/zenodo.5727117>

- Boyden, P, Weil-Accardo, J, Deschamps, P, Oppo, D and Rovere, A.** 2021. Last interglacial sea-level proxies in East Africa and the Western Indian Ocean. *Earth System Science Data*, 13: 1633–1651. DOI: <https://doi.org/10.5194/essd-13-1633-2021>
- Braithwaite, CJ.** 2020. Last Interglacial changes in sea level on Aldabra, western Indian Ocean. *Sedimentology*. DOI: <https://doi.org/10.1111/sed.12738>
- Braithwaite, CJ, Taylor, J and Kennedy, WJ.** 1973. The evolution of an atoll: the depositional and erosional history of Aldabra, *Philosophical Transactions of the Royal Society of London. Biological Sciences*, 266: 307–340, DOI: <https://doi.org/10.1098/rstb.1973.0051>
- Camoin, GF, Montaggioni, LF and Braithwaite, CJR.** 2004. Late glacial to post glacial sea levels in the Western Indian Ocean. *Marine Geology*, 206: 119–146. DOI: <https://doi.org/10.1016/j.margeo.2004.02.003>
- Casella, E, Collin, A, Harris, D, Ferse, S, Bejarano, S, Parravicini, V, Hench, JL and Rovere, A.** 2017. Mapping coral reefs using consumer-grade drones and structure from motion photogrammetry techniques. *Coral Reefs*, 36: 269–275. DOI: <https://doi.org/10.1007/s00338-016-1522-0>
- Cerrone, C, Vacchi, M, Fontana, A and Rovere, A.** 2021. Last Interglacial sea-level proxies in the Western Mediterranean. *Earth System Science Data Discussions*, 2021: 1–93. DOI: <https://doi.org/10.5194/essd-2021-49>
- Chappell, J and Shackleton, N.** 1986. Oxygen isotopes and sea level. *Nature*, 324: 137–140. DOI: <https://doi.org/10.1038/324137a0>
- Chen, JH, Ccurran, HA, White, B and Wasserburg, GJ.** 1991. Precise chronology of the last interglacial period:  $^{234}\text{U}$ - $^{230}\text{Th}$  data from fossil coral reefs in the Bahamas. *GSA Bulletin*, 103: 82–97. DOI: [https://doi.org/10.1130/0016-7606\(1991\)103<0082:PCOTLI>2.3.CO;2](https://doi.org/10.1130/0016-7606(1991)103<0082:PCOTLI>2.3.CO;2)
- Cheng, H, Edwards, RL, Shen, C.-C, Polyak, VJ, Asmerom, Y, Woodhead, J, Hellstrom, J, Wang, Y, Kong, X, Spötl, C, et al.** 2013. Improvements in  $^{230}\text{Th}$  dating,  $^{230}\text{Th}$  and  $^{234}\text{U}$  half-life values, and U–Th isotopic measurements by Multi-Collector Inductively Coupled Plasma Mass Spectrometry. *Earth and Planetary Science Letters*, 371: 82–91. DOI: <https://doi.org/10.1016/j.epsl.2013.04.006>
- Chiang, H-W, Lu, Y, Wang, X, Lin, K and Liu, X.** 2019. Optimizing MC-ICP-MS with SEM protocols for determination of U and Th isotope ratios and  $^{230}\text{Th}$  ages in carbonates. *Quaternary Geochronology*, 50: 75–90. DOI: <https://doi.org/10.1016/j.quageo.2018.10.003>
- Chutcharavan, PM and Dutton, A.** 2021. A global compilation of U-series-dated fossil coral sea-level indicators for the Last Interglacial period (Marine Isotope Stage 5e). *Earth System Science Data*, 13: 3155–3178. DOI: <https://doi.org/10.5194/essd-13-3155-2021>
- Codignotto, JO, Marcomini, SC and Santillana, SN.** 1988. Terrazas marinas entre Puerto Deseado y Bahía Bustamante, Santa Cruz, Chubut. *Revista de la Asociación Geológica Argentina*, 43: 43–50.
- Creveling, JR, Mitrovica, JX, Clark, PU, Waelbroeck, C and Pico, T.** 2017. Predicted bounds on peak global mean sea level during marine isotope stages 5a and 5c. *Quaternary Science Reviews*, 163: 193–208. DOI: <https://doi.org/10.1016/j.quascirev.2017.03.003>
- Creveling, JR, Mitrovica, JX, Hay, CC, Austermann, J and Kopp, RE.** 2015. Revisiting tectonic corrections applied to Pleistocene sea-level highstands. *Quaternary Science Reviews*, 111: 72–80. DOI: <https://doi.org/10.1016/j.quascirev.2015.01.003>
- Cuttler, MV, Hansen, JE, Lowe, RJ, Trotter, JA and McCulloch, MT.** 2019. Source and supply of sediment to a shoreline salient in a fringing reef environment. *Earth Surface Processes and Landforms*, 44: 552–564. DOI: <https://doi.org/10.1002/esp.4516>
- Dendy, S, Austermann, J, Creveling, J and Mitrovica, JX.** 2017. Sensitivity of Last Interglacial sea-level high stands to ice sheet configuration during Marine Isotope Stage 6. *Quaternary Science Reviews*, 171: 234–244. DOI: <https://doi.org/10.1016/j.quascirev.2017.06.013>
- Deschamps, P, Durand, N, Bard, E, Hamelin, B, Camoin, G, Thomas, AL, Henderson, GM, Okuno, J and Yokoyama, Y.** 2012. Ice-sheet collapse and sea-level rise at the Bølling warming 14,600 years ago. *Nature*, 483: 559–564. DOI: <https://doi.org/10.1038/nature10902>
- Du Puy, D and Moat, J.** 1996. A refined classification of the primary vegetation of Madagascar based on the underlying geology: using GIS to map its distribution and to assess its conservation status. *Biogéographie de Madagascar*, 1996: 205–218.
- Dutton, A and Lambeck, K.** 2012. Ice Volume and Sea Level During the Last Interglacial. *Science*, 337: 216–219. DOI: <https://doi.org/10.1126/science.1205749>
- Dutton, A, Webster, JM, Zwart, D, Lambeck, K and Wohlfarth, B.** 2015. Tropical tales of polar ice: evidence of Last Interglacial polar ice sheet retreat recorded by fossil reefs of the granitic Seychelles islands. *Quaternary Science Reviews*, 107: 182–196. DOI: <https://doi.org/10.1016/j.quascirev.2014.10.025>
- Gallup, CD, Edwards, RL and Johnson, RG.** 1994. The timing of high sea levels over the past 200,000 years. *Science*, 263: 796–800. DOI: <https://doi.org/10.1126/science.263.5148.796>
- Gowan, EJ, Rovere, A, Ryan, DD, Richiano, S, Montes, A, Pappalardo, M and Aguirre, ML.** 2021. Last interglacial (MIS 5e) sea-level proxies in southeastern South America. *Earth System Science Data*, 13: 171–197. DOI: <https://doi.org/10.5194/essd-13-171-2021>
- Gvrtzman, G.** 1994. Fluctuations of sea level during the past 400 000 years: the record of Sinai, Egypt (northern Red Sea). *Coral Reefs*, 13: 203–214. DOI: <https://doi.org/10.1007/BF00303633>
- Hallmann, N, Camoin, G, Webster, JM and Humblet, M.** 2021. A standardized database of Marine Isotopic Stage 5e sea-level proxies on tropical Pacific Islands. *Earth System Science Data*, 13: 2651–2699. DOI: <https://doi.org/10.5194/essd-13-2651-2021>



- Hearty, PJ, Miller, GH, Stearns, CE and Szabo, BJ.** 1986. Aminostratigraphy of Quaternary shorelines in the Mediterranean basin. *Geological Society of America Bulletin*, 97: 850–858. DOI: [https://doi.org/10.1130/0016-7606\(1986\)97<850:AOQSIT>2.0.CO;2](https://doi.org/10.1130/0016-7606(1986)97<850:AOQSIT>2.0.CO;2)
- Hibbert, FD, Rohling, EJ, Dutton, A, Williams, FH, Chutcharavan, PM, Zhao, C and Tamisiea, ME.** 2016. Coral indicators of past sea-level change: A global repository of U-series dated benchmarks. *Quaternary Science Reviews*, 145: 1–56. DOI: <https://doi.org/10.1016/j.quascirev.2016.04.019>
- Jaffey, A, Flynn, K, Glendenin, L, Bentley, WT and Essling, A.** 1971. Precision measurement of half-lives and specific activities of U 235 and U 238. *Physical review C*, 4: 1889. DOI: <https://doi.org/10.1103/PhysRevC.4.1889>
- Mauz, B, Vacchi, M, Green, A, Hoffmann, G and Cooper, A.** 2015. Beachrock: a tool for reconstructing relative sea level in the far-field. *Marine Geology*, 362: 1–16. DOI: <https://doi.org/10.1016/j.margeo.2015.01.009>
- McLean, RF.** 1967. Origin and development of ridge-furrow systems in beachrock in Barbados, West Indies. *Marine Geology*, 5: 181–193. DOI: [https://doi.org/10.1016/0025-3227\(67\)90080-1](https://doi.org/10.1016/0025-3227(67)90080-1)
- Montaggioni, LF.** 1972. Essai de chronologie relative des stationnements marins quaternaires à l'île Maurice (Archipel des Mascareignes, Ocean Indien). *CR. Acad. Sci. Paris, D*, 274: 2936–2939.
- Montaggioni, LF and Braithwaite, CJ.** 2009. Quaternary coral reef systems: history, development processes and controlling factors, Elsevier.
- National Oceanic and Atmospheric Administration.** 2019. Tide Tables 2019 Central and Western Pacific Ocean and Indian Ocean, Center for Operational Oceanographic Products and Services, Silver Spring, MD, USA.
- Nichols, G.** 2009. Sedimentology and Stratigraphy, John Wiley & Sons, Incorporated, Hoboken, United Kingdom.
- Roberts, DL, Karkanis, P, Jacobs, Z, Marean, CW and Roberts, RG.** 2012. Melting ice sheets 400,000 yr ago raised sea level by 13 m: Past analogue for future trends. *Earth and Planetary Science Letters*, 357: 226–237. DOI: <https://doi.org/10.1016/j.epsl.2012.09.006>
- Rovere, A, Raymo, ME, Vacchi, M, Lorscheid, T, Stocchi, P, Gómez-Pujol, L, Harris, DL, Casella, E, O'Leary, MJ and Hearty, PJ.** 2016. The analysis of Last Interglacial (MIS 5e) relative sea-level indicators: Reconstructing sea-level in a warmer world. *Earth-Science Reviews*, 159: 404–427. DOI: <https://doi.org/10.1016/j.earscirev.2016.06.006>
- Seddon, N, Tobias, J, Yount, JW, Ramanampamonjy, JR, Butchart, S and Randrianizahana, H.** 2000. Conservation issues and priorities in the Mikea Forest of south-west Madagascar. *Oryx*, 34: 287–304. DOI: <https://doi.org/10.1046/j.1365-3008.2000.00134.x>
- Sepulcre, S, Durand, N and Bard, E.** 2009. Mineralogical determination of reef and periplatform carbonates: calibration and implications for paleoceanography and radiochronology. *Global and Planetary Change*, 66: 1–9. DOI: <https://doi.org/10.1016/j.gloplacha.2008.07.008>
- Stephenson, SN, White, NJ, Li, T and Robinson, LF.** 2019. Disentangling interglacial sea level and global dynamic topography: Analysis of Madagascar. *Earth and Planetary Science Letters*, 519: 61–69. DOI: <https://doi.org/10.1016/j.epsl.2019.04.029>
- Taviani, M, Montagna, P, Rasul, NM, Angeletti, L and Bosworth, W.** 2019. Pleistocene coral reef terraces on the Saudi Arabian side of the Gulf of Aqaba. *Red Sea*, pp. 341–365. Springer. DOI: [https://doi.org/10.1007/978-3-319-99408-6\\_16](https://doi.org/10.1007/978-3-319-99408-6_16)
- Thompson, WG, Spiegelman, MW, Goldstein, SL and Speed, RC.** 2003. An open-system model for U-series age determinations of fossil corals. *Earth and Planetary Science Letters*, 210: 365–381. DOI: [https://doi.org/10.1016/S0012-821X\(03\)00121-3](https://doi.org/10.1016/S0012-821X(03)00121-3)
- Thurber, DL, Broecker, WS, Blanchard, RL and Potratz, HA.** 1965. Uranium-series ages of Pacific atoll coral. *Science*, 149: 55–58. DOI: <https://doi.org/10.1126/science.149.3679.55>
- Tierney, JE, Poulsen, CJ, Montañez, IP, Bhattacharya, T, Feng, R, Ford, HL, Hönisch, B, Inglis, GN, Petersen, SV, Sagoo, N, Tabor, CR, Thirumalai, K, Zhu, J, Burls, NJ, Foster, GL, Goddérís, Y, Huber, BT, Ivany, LC, Kirtland Turner, S, Lunt, DJ, McElwain, JC, Mills, BJW, Otto-Bliesner, BL, Ridgwell, A and Zhang, YG.** 2020. Past climates inform our future. *Science*, 370. DOI: <https://doi.org/10.1126/science.aay3701>
- Vermeesch, P.** 2018. IsoplotR: A free and open toolbox for geochronology. *Geoscience Frontiers*, 9: 1479–1493. DOI: <https://doi.org/10.1016/j.gsf.2018.04.001>
- Villemant, B and Feuillet, N.** 2003. Dating open systems by the 238U–234U–230Th method: application to Quaternary reef terraces. *Earth and Planetary Science Letters*, 210: 105–118. DOI: [https://doi.org/10.1016/S0012-821X\(03\)00100-6](https://doi.org/10.1016/S0012-821X(03)00100-6)
- Vyverberg, K, Dechnik, B, Dutton, A, Webster, JM, Zwart, D and Portell, RW.** 2018. Episodic reef growth in the granitic Seychelles during the Last Interglacial: implications for polar ice sheet dynamics. *Marine Geology*, 399: 170–187. DOI: <https://doi.org/10.1016/j.margeo.2018.02.010>
- Woodworth, PL.** 2017. Differences between mean tide level and mean sea level. *Journal of Geodesy*, 91: 69–90. DOI: <https://doi.org/10.1007/s00190-016-0938-1>
- Yan, Q, Korty, R, Wei, T and Jiang, N.** 2021. A Westward Shift in Tropical Cyclone Potential Intensity and Genesis Regions in the North Atlantic During the Last Interglacial. *Geophysical Research Letters*, 48. DOI: <https://doi.org/10.1029/2021GL093946>
- Yeung, NK-H, Menviel, L, Meissner, KJ, Taschetto, AS, Ziehn, T and Chamberlain, M.** 2021. Land–sea temperature contrasts at the Last Interglacial and their impact on the hydrological cycle. *Climate of the Past*, 17: 869–885. DOI: <https://doi.org/10.5194/cp-17-869-2021>

---

**TO CITE THIS ARTICLE:**

Boyden, P, Weil-Accardo, J, Deschamps, P, Godeau, N, Jaosedy, N, Guihou, A, Rajaonarivelo, MN, O'Leary, M, Humblet, M and Rovere, A. 2022. Revisiting Battistini: Pleistocene Coastal Evolution of Southwestern Madagascar. *Open Quaternary*, 8: 14, pp.1–17. DOI: <https://doi.org/10.5334/oq.112>

**Submitted:** 14 December 2021    **Accepted:** 01 June 2022    **Published:** 27 December 2022

**COPYRIGHT:**

© 2022 The Author(s). This is an open-access article distributed under the terms of the Creative Commons Attribution 4.0 International License (CC-BY 4.0), which permits unrestricted use, distribution, and reproduction in any medium, provided the original author and source are credited. See <http://creativecommons.org/licenses/by/4.0/>.

*Open Quaternary* is a peer-reviewed open access journal published by Ubiquity Press.

